Annular Bragg Defect Mode Resonators

Jacob Scheuer*[a], William M. J. Green[b], Guy DeRose[a,b] and Amnon Yariv[a,b]
[a] Dept. of Applied Physics, California Inst. of Technology, 1200 E. California Blvd., Pasadena, CA USA 91125
[b] Dept. of Electrical Engineering, California Inst. of Technology, 1200 E. California Blvd., Pasadena, CA USA 91125

ABSTRACT

We propose and analyze a new type of resonator in an annular geometry which is based on a single defect surrounded by radial Bragg reflectors on both sides. Unlike conventional, total internal reflection based ring resonators, this structure supports modal fields with very low azimuthal number (large radial k-vector component). We show that the conditions for efficient mode confinement are different from those of conventional Bragg waveguiding in a rectangular geometry. To realize tight confinement of the light in the defect, chirped gratings are required. Compared to a conventional resonator, the new resonator exhibits larger FSR and lower losses making it suitable for both telecom and sensing applications. In addition, the resonance wavelength and Q factor of the device are very sensitive to environmental changes, and thus provide ideal observables for sensing applications. Annular Bragg resonators with several unique geometries have been fabricated in an InGaAsP multi-quantum-well membrane. The spectral properties of the resonators have been investigated through analysis of photoluminescence induced by pulsed optical excitation.
Keywords:

1. INTRODUCTION

Circular optical resonators (rings, disks and spheres) have been investigated since the late 1960's[1]. In the last three decades, numerous applications utilizing annular resonators for optical communication and sensing have been suggested, analyzed, and demonstrated. More recently, as fabrication and material technologies have matured, much effort was devoted to improving the characteristics of these resonators, and to realizing higher Q-factors and larger free spectral ranges (FSRs).

Most of the previously studied optical resonators (i.e., "conventional" resonators), utilized total internal reflection (TIR) to attain confinement of the modal field in a guiding core[2]. In order to exploit TIR, the refractive index of the resonator structure must be higher than the refractive index of its surroundings. Such configuration, however, introduces limitations on the properties of the modal field such as loss per revolution and the maximal possible radial wavenumber which, in turn, limit the maximal realizable FSR and Q-factor.

Circular resonators have been shown to be very useful for telecommunication and sensing applications[2]. The potential application of conventional, TIR based, ring resonators in the fields of telecommunication[2] and sensing[3] have been studied and demonstrated. For both types of applications, compact and high-Q (low loss) resonators with a single radial (transverse) mode and large FSR are desired. For sensing applications, high sensitivity to changes in the environment surrounding the resonator is also required, in order to enable the detection of small environmental fluctuations. For example, such fluctuations could include changes in the concentration of a liquid or gas species in which the resonator in immersed, in chemical or biological sensing applications.

* koby@caltech.edu; phone 1 626 395-4413; fax 1 626 405-0928; www.its.caltech.edu/~koby/

In this paper we propose and analyze a new type of ring resonator - an annular defect mode resonator which is based on a single annular defect located between radial Bragg reflectors[4-6]. In this resonator, Bragg reflection is utilized as the radial confinement mechanism instead of TIR. Bragg reflection is not subject to the limitations of TIR (refractive index demands, critical angle etc.) and, therefore, supports modal fields which cannot evolve in conventional resonators. Bragg reflection based disk resonators (i.e., a disk surrounded by concentric Bragg layers) have been studied theoretically and demonstrated experimentally[7-15]. Recently, a hexagonal waveguide ring resonator based on Photonic Bandgap Crystal (PBC) confinement on both sides of the waveguide was demonstrated experimentally[16]. However, this structure exploited the specific symmetry of the triangular lattice which enables low loss 60° abrupt turns, in order to realize a closed resonator.

2. BASIC THEORY

We consider an azimuthally symmetric structure as illustrated in Figure 1. The guiding defect, which is comprised of a material of refractive index n_{defect}, is surrounded by distributed Bragg reflectors on both sides, where the reflectors' layers are of refractive indices n_1 and n_2. All the electromagnetic field components can be expressed in terms of the z-component of the electric and magnetic fields.[17] These satisfy the Helmholtz equation which in cylindrical coordinates is given by:

$$\left[\rho^2\frac{\partial^2}{\partial\rho^2}+\rho\frac{\partial}{\partial\rho}+\left(k^2(\rho)-\beta^2\right)\rho^2-m^2\right]\begin{pmatrix}E_z\\H_z\end{pmatrix}=0 \tag{1}$$

where ρ and θ are the radial and azimuthal coordinates respectively, m is the azimuthal wavenumber, β is the z-component propagation coefficient, $k(\rho) = k_0 \cdot n(\rho)$, k_0 is the wavenumber in vacuum, and the refractive index $n(\rho)$ equals either n_{defect}, n_1, or n_2 according to the radius ρ.

The general solution of equation (1) can be expressed by a superposition of the Bessel functions of the first and second kind.

$$\begin{aligned}E_z &= \left[A\cdot J_m\left(\sqrt{k_j^2-\beta^2}\,\rho\right)+B\cdot Y_m\left(\sqrt{k_j^2-\beta^2}\,\rho\right)\right]\cdot\cos(\beta\cdot z+\varphi)\cdot\exp(im\theta)\\ H_z &= \left[C\cdot J_m\left(\sqrt{k_j^2-\beta^2}\,\rho\right)+D\cdot Y_m\left(\sqrt{k_j^2-\beta^2}\,\rho\right)\right]\cdot\sin(\beta\cdot z+\varphi)\cdot\exp(im\theta)\end{aligned} \tag{2}$$

where k_j is the material wavenumber in the j^{th} layer.

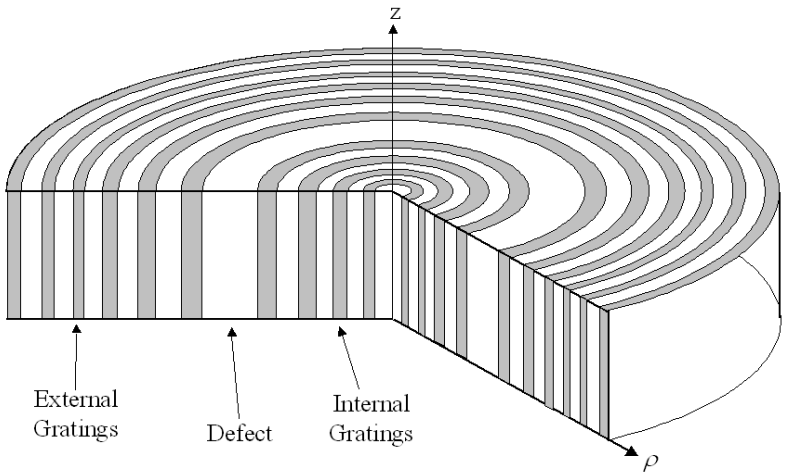

Figure 1. An illustration of the annular defect mode resonator structure.

The other field components can be easily derived from E_z and H_z[17]. Introducing (2) into (3) yields all the field components in the j^{th} layer. The tangential component of the fields – E_z, H_z, E_θ, H_θ – must be continuous at the interfaces. This requirement can be written in the form of a transfer matrix, connecting the amplitude vector [A B C D] in the j^{th} and j+1 layers. In this paper we consider ring resonator modes which propagate primarily in the azimuthal direction, having $\beta \approx 0$. In this case there are two independent types of solutions – a TE mode with E_z, H_ρ, and H_θ and a TM mode with H_z, E_ρ, and E_θ. We consider the "TE" component of the electromagnetic field which is characterized by E_z, H_ρ and H_θ. The tangential components of the field in the j^{th} layer are given by:

$$\begin{pmatrix} E_z \\ H_\theta \end{pmatrix}_j = \begin{pmatrix} J(\gamma_j \rho) & Y(\gamma_j \rho) \\ \frac{n_j^2}{\gamma_j} J'(\gamma_j \rho) & \frac{n_j^2}{\gamma_j} Y'(\gamma_j \rho) \end{pmatrix} \begin{pmatrix} A_j \\ B_j \end{pmatrix} = \overline{M}_j \begin{pmatrix} A_j \\ B_j \end{pmatrix} \tag{3}$$

where $\gamma_j = \sqrt{k_j^2 - \beta^2}$, A and B are the same as in (2), J and Y are the Bessel functions of the first and second kind and the prime indicates a derivative with respect to the function argument. The continuity of the tangential fields at the boundary separating adjacent layers leads to:

$$\begin{pmatrix} A_{j+1} \\ B_{j+1} \end{pmatrix} = \overline{M}_{j+1}^{-1} \cdot \overline{M}_j \begin{pmatrix} A_j \\ B_j \end{pmatrix} \tag{4}$$

Using relation (3), the field components A and B can be "propagated" from the inner layers to the external layers. We use the finiteness of the field at $\rho = 0$ so that $B_1 = 0$. The second boundary condition is that past the last layer there is no inward propagating field so that $B_{N+1} = -iA_{N+1}$ (for the TE mode) and N is the number of layers.

3. STRUCTURE DESIGN

3.1. First-Order Bragg reflectors

The formalism of Section 2 enables us to find the modal field distribution in the case of an arbitrary arrangement of annular concentric dielectric rings. We are especially interested in structures that can lead to a concentration of the modal energy near a predetermined radial distance i.e., in a radial defect mode.

High efficiency Bragg reflectors in Cartesian coordinates require a constant grating period which determines the angles in which an incident wave would be reflected. Generally, the grating wavenumber ($2\pi/\Lambda$ where Λ is the grating period) multiplied by the reflection order should be approximately twice the transverse component of the incident wave's wavevector[17]. However, when the structure possesses cylindrical symmetry, the conditions for efficient reflection are different.

Several methods for determining the thickness, and thus the position, of the Bragg layer interfaces have been suggested in previous publications[9-11]. Compared to Bragg fibers[18], the incident angle of the waves at the interfaces (measured from the normal to the interface) is smaller. Therefore, the asymptotic approximation[19,20] is invalid and the "conventional" $\lambda/4$ layers would not be appropriate. The principle underlying these methods is to position the interfaces between the layers at the zeros and extrema of the transverse field profile. Practically, this procedure generates effective "$\lambda/4$" layers, layers which have the width of a quarter of the radial oscillation period. However, since the radial field profile is a superposition of Bessel functions, this periodicity is not constant and the resulting layers are no longer equally spaced (see also Figure 3). This strategy ensures the decrease of the field intensity for larger radii and the reduction of radiating power from the resonator.

Figure 2 depicts the index (A) and the modal field (B) profiles of an annular defect mode resonator. The high index layers have effective refractive index ($\overline{n}$) of 2 while the low index layers and the defect have effective refractive index

of 1. The internal and external Bragg reflectors have 5 and 10 periods respectively, the resonant wavelength is 1.55 μm and the azimuthal wavenumber is 7. The defect is located approximately at $\rho = 5.6$ μm and is 0.85 μm wide.

Figure 3 shows the width of the high-index (stars) and low-index (circles) layers. Unlike regular Bragg (or photonic crystal) waveguides in Cartesian coordinates, the required gratings are chirped. At small radii the layers are wider due to the characteristics of the Bessel function, which exhibits lower oscillation frequency at small radii. The layers widths decrease for larger radii, asymptotically approaching the "conventional" quarter wavelength width $\lambda/4n$. The two exceptionally wider low-index layers in Figure 3 are the first low-index layer ($\rho = 0$-2 μm) and the low-index defect which has a width of $\lambda/2$.

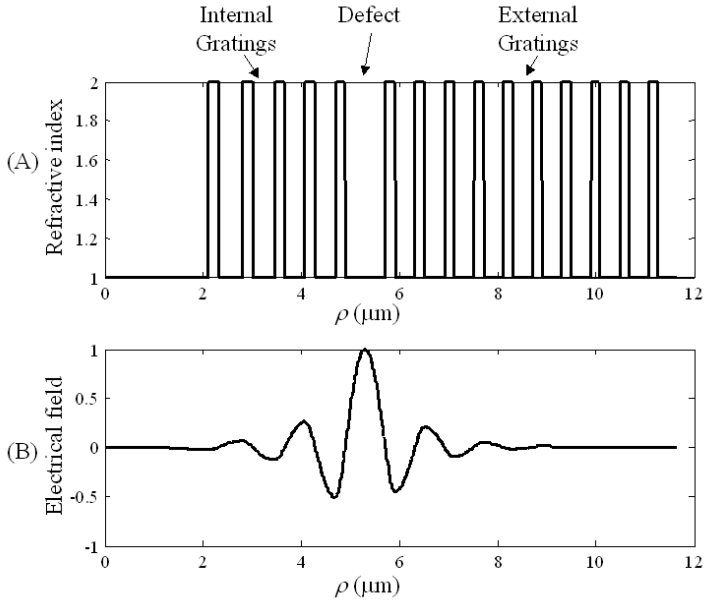

Figure 2. Radial index profile (A) and electric field (E_z) distribution (B) of an annular defect mode resonator.

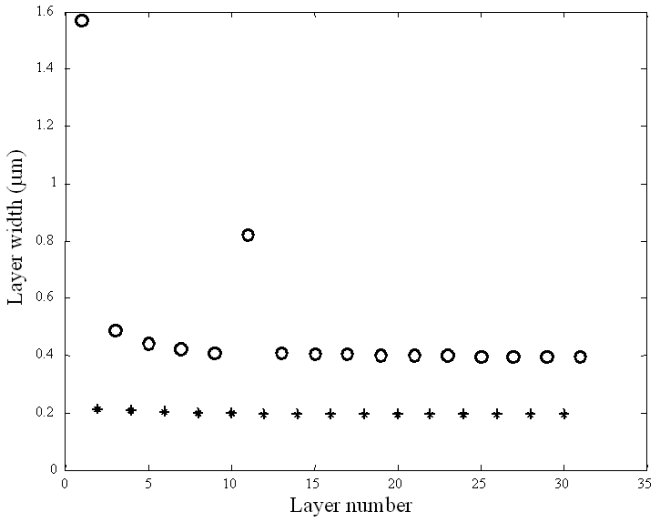

Figure 3. The high-index (stars) and low-index (circles) layer widths of the resonator shown in Figure 2.

3.2. Higher Bragg-order reflectors

Although the structure consisting of chirped quarter-wavelength Bragg layers forms an optimal reflector, its implementation could prove to be difficult. Because the layers' spatial period changes, some of the conventional photolithography methods which are employed for generation of uniformly spaced Bragg gratings[21] cannot be used. This introduces tight demands on fabrication accuracy and tolerances. A possible approach to overcome this problem is to position the interfaces in non-sequential zeros/extrema, i.e. allow the Bessel function in each layer to complete a full period before changing the index. From the Bragg reflection point of view, such an approach is equivalent to utilizing layers of thickness $(2l+1)\lambda/4n$, where l is a positive integer, or employing higher reflection orders of the Bragg stack.

The resulting structure would have wider layers and would, therefore, be larger and exhibit smaller FSR. Figure 4 compares the transverse field profile of the structure in Figure 2 (4A) and the transverse profile of a resonator designed for similar mode parameters (5 internal periods, 10 external periods, $m = 7$ for $\lambda = 1.55$ μm) utilizing wider layers (4B). The radius at which the field amplitude peaks is more than twice larger than the original (11.35 μm vs. 5.6 μm) and the radial decay rate of the field is smaller.

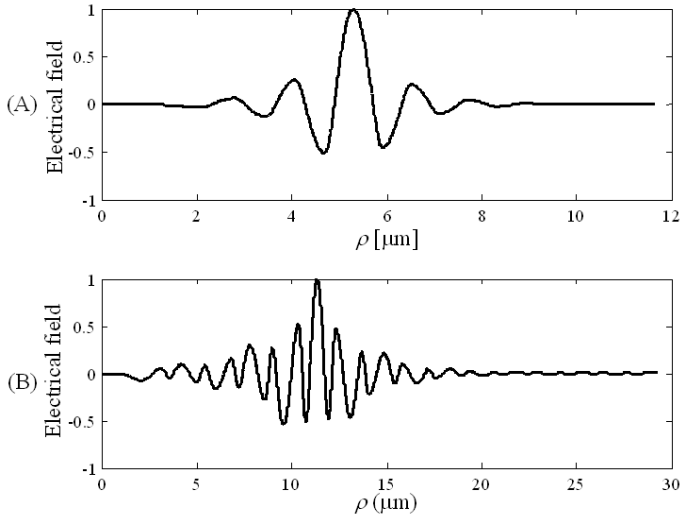

Figure 4. A comparison of the modal field profile shown in Figure 2 (4A) and the modal field of a resonator based on second-order Bragg reflectors with similar parameters (4B).

Figure 5 compares the dispersion curve of the higher-order Bragg based resonator (B) to the dispersion curve of the first-order design (A). As expected, the FSR of the higher-order Bragg based resonator is significantly smaller than that of the original one (approximately 3 nm at 1.55 μm compared to ~20 nm for first order). The main reason for this decrease in the FSR is the increase in the defect radius. However, the FSR can be increased by using a composite Bragg reflector in which the low and high index layers employ different Bragg order. Since the lower index layers are inherently wider (especially in the lower radii regime), they can be realized utilizing quarter wavelength layers, while the high-index layers remain as a higher order Bragg layer. Moreover, depending on the radius and the index, the Bragg order of each layer could be determined separately to achieve the largest FSR.

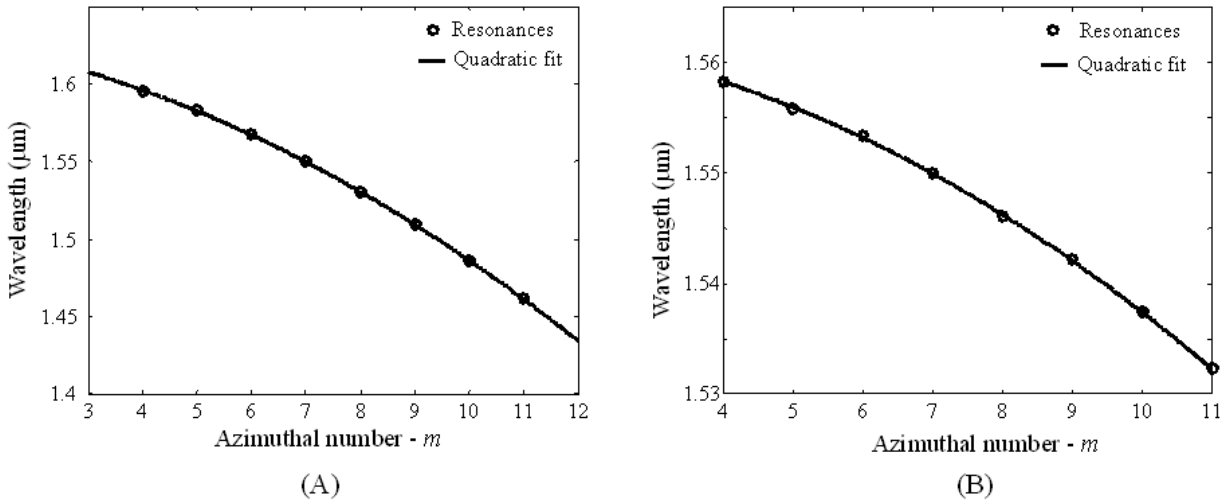

Figure 5. Comparison between the dispersion curves of an annular defect resonator employing first order (A) and second order (B) Bragg reflectors.

4. DEVICE FABRICATION

Annular Bragg resonators of several geometries and Bragg reflector orders were fabricated within a thin membrane of InGaAsP semiconductor material. A cross-section of the semiconductor epitaxial structure used is illustrated in Figure 6. The layers were grown by MOCVD on a (100) oriented InP substrate. This structure consists of a 500nm thick InP buffer layer, followed by a 50 nm InGaAsP (λ_g = 1.3μm) stop etch, and a 250nm InP sacrificial layer. A 250nm membrane composed of 605 Å InGaAsP (λ_g = 1.1μm) layers sandwiching six 75Å quantum wells (1% compressive strain) separated by 120 Å InGaAsP barriers (λ_g = 1.2μm, 0.5% tensile strain) completes the structure. Photoluminescence from the quantum wells peaks at a wavelength λ = 1559nm. Annular Bragg resonators were designed to have resonant wavelengths between 1.5-1.6μm, for large overlap with the gain spectrum of the multi-quantum-well material.

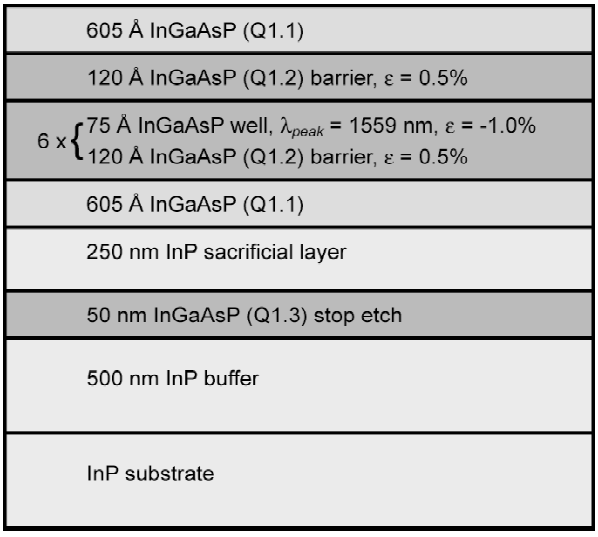

Figure 6. InGaAsP/InP multi-quantum-well semiconductor structure.

The optical gain of the semiconductor epitaxial structure used favors the TM polarization (H_z), because of the optical properties of compressively strained quantum wells[22]. The design and analysis of resonators for this polarization is similar to the TE case where, instead of equation (3), we use the TM boundary conditions:

$$\begin{pmatrix} H_z \\ E_\theta \end{pmatrix}_j = \begin{pmatrix} J(\gamma_j \rho) & Y(\gamma_j \rho) \\ \frac{1}{\gamma_j} J'(\gamma_j \rho) & \frac{1}{\gamma_j} Y'(\gamma_j \rho) \end{pmatrix} \begin{pmatrix} C_j \\ D_j \end{pmatrix} = \overline{M}_j \begin{pmatrix} C_j \\ D_j \end{pmatrix} \quad (5)$$

In addition, we used the effective index method[23] in order to reduce the 3-dimensional problem to a 2-dimentional one. For the fabricated device, the effective indices of refraction of the high-index and low-index layers are approximately 2.8 and 1.54 respectively.

The procedure followed to fabricate the annular Bragg resonators is as follows. First, an etch mask consisting of 120 nm of PECVD SiO_2 was deposited on the semiconductor substrate. A 550 nm thick layer of PMMA electron-sensitive resist was spin-coated onto the substrate, and electron beam lithography was perfomed with a Leica EBPG 5000 direct-write system, to define the resonator patterns in the PMMA. The patterns were then transferred to the SiO_2 layer with a reactive ion etching (RIE) step in C_4F_8 plasma, after which the remaining PMMA was stripped using O_2 plasma. A second RIE step was used to transfer the SiO_2 pattern through the 250 nm thick InGaAsP membrane and approximately 75 nm into the InP sacrificial layer, using HI/H2/Ar plasma. Finally, the remaining SiO_2 etch mask was removed with a buffered hydrofluoric acid wet chemical etch.

The high refractive index of the InP substrate ($n \approx 3.17$ at $\lambda = 1.55$ μm) on which the InGaAsP membrane is grown drastically reduces the vertical confinement of the guided optical mode within the membrane. Therefore, in order to achieve strong vertical optical confinement and improve the quality factor Q of the resonators, the patterned InGaAsP membrane must be surrounded by low index material. One method for achieving this is to generate an air-suspended membrane by selective removal of the InP beneath the device, as is commonly done with photonic crystal devices[24]. However, this technique is not applicable to the resonators studied here, because the concentric ring structure would collapse if the solid substrate were removed. Therefore, the resonators were flip-bonded to a double-side polished sapphire substrate with a thin layer of UV curable optical adhesive (Norland NOA 73, $n \approx 1.54$ at $\lambda = 1.55$ μm). After fully curing the adhesive under a UV lamp, the InP substrate was removed using a combination of mechanical lapping and selective chemical etching. Note that the excellent thermal properties of sapphire can improve the conduction of heat generated during optical pumping away from the membrane. In addition, the large bandgap energy of sapphire, and associated transparency at visible and infrared wavelengths, permits optical pumping and imaging of the resonator luminescence from either the top or bottom of the device. Transfer of the semiconductor membrane to a transparent substrate also facilitates use of annular Bragg resonators for sensing applications. For instance, a solution containing an analyte whose concentration is to be monitored by the resonator could be introduced via the exposed top side of the device, while optical pumping of the resonator and imaging of the sensor signal could be accomplished through the transparent substrate.

Scanning electron microscope images of several completed devices are shown in Figure 8, prior to transfer of the InGaAsP membrane to the sapphire substrate. The images were taken at a tilt angle of ~70° with respect to the substrate surface normal, therefore the circular resonators appear elliptical. Images (A)-(C) show annular Bragg resonators with defect widths of $\lambda/2n$, $3\lambda/2n$, and $5\lambda/2n$ respectively. Odd-order defects were chosen to maximize modal overlap with the gain profile in the defect. A close examination of each reveals that the period of the Bragg gratings decreases moving radially outward from the center, as is required by the optimal design. The magnified view of the InGaAsP ridges in image (D) illustrates the very smooth vertical sidewalls achieved with our RIE process, which will minimize scattering of the strongly confined optical modes.

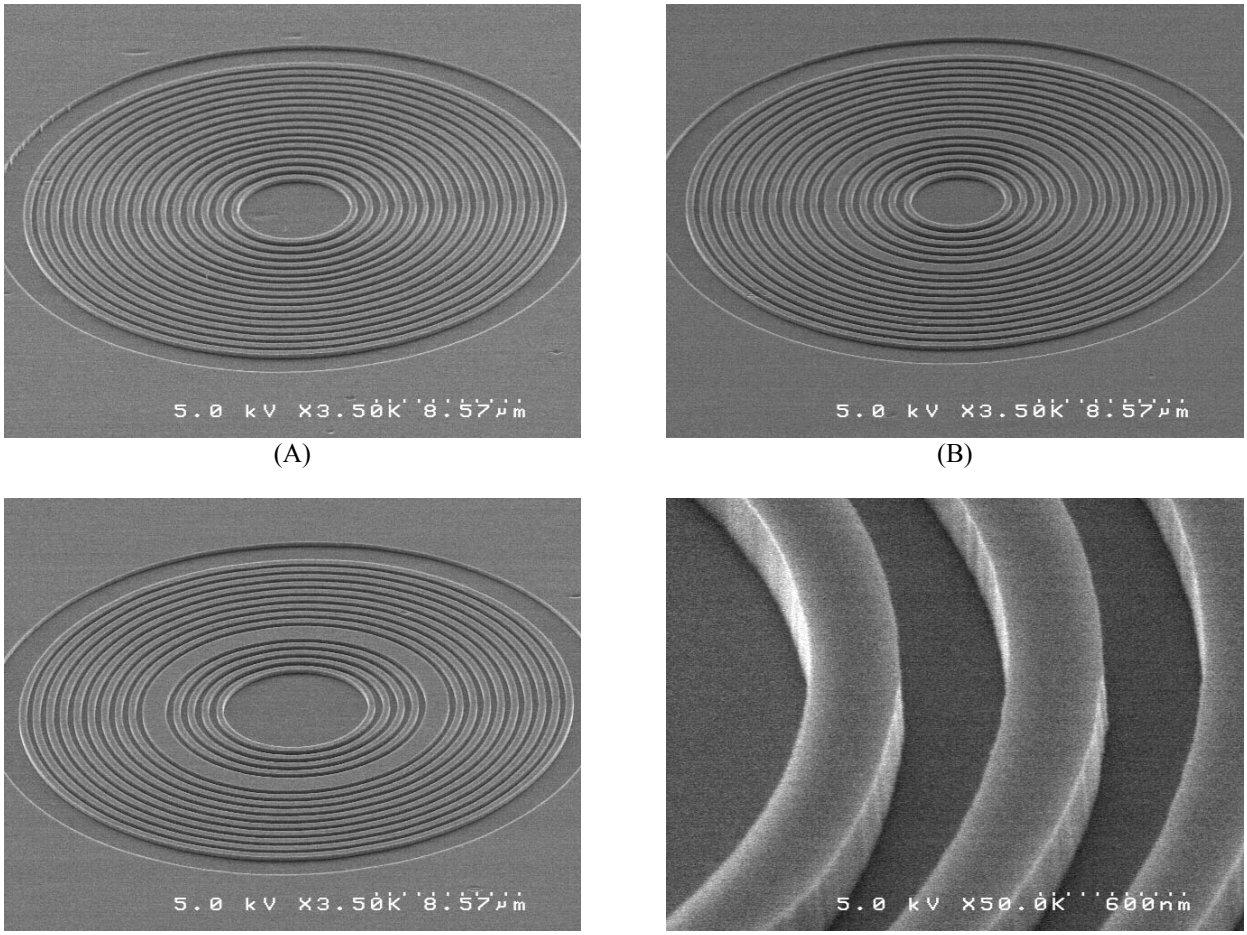

(A) (B)

(C) (D)

Figure 8. SEM images of completed annular Bragg resonators, taken after RIE through the InGaAsP membrane. All devices have $\lambda/4n$ wide (1st order) low index layers, and $3\lambda/4n$ wide (2nd order) high index layers. (A) $\lambda/2n$ defect. (B) $3\lambda/2n$ defect. (C) $5\lambda/2n$ defect. (D) Magnified image of $3\lambda/4n$ wide InGaAsP ridges, illustrating smooth vertical sidewalls.

5. MEASUREMENT RESULTS

We measured and analyzed the vertical emission from the resonators under pulsed optical pumping. Figure 9(A) shows a schematic of the measurement configuration: A Ti:sapphire mode-locked laser was used to optically pump the devices at a center wavelength of 891 nm, repetition rate of 76.3 MHz and pulse duration of approximately 100 fs. A variable attenuator was used to control the pump power. The average pump power and center wavelength were monitored by a wavemeter, through a 50/50 beamsplitter. A 20x long-working-distance microscope objective (NA = 0.42) was used to focus the pump onto the annular Bragg resonators and to collect the emitted radiation from the devices. The position of the focal plane was varied to adjust the pump spot size at the sample surface, illuminating either a broad or restricted region of a single resonator, as illustrated in Figure 9(B). Positioning of the resonators under the pump spot was achieved using a high-precision mechanical stage with piezoelectric actuators. The photoluminescence signal was focused into a multimode fiber connected to an optical spectrum analyzer which was used to measure the power spectrum of the photoluminescence. Alternatively, the photoluminescence signal could be imaged by an infrared vidicon camera (after filtration of the pump reflected from the sample), by redirecting the signal with a flip-up mirror. A CCD camera was also

positioned to image the resonators and the pump spot, for alignment purposes, using a white light source and a second flip-up mirror.

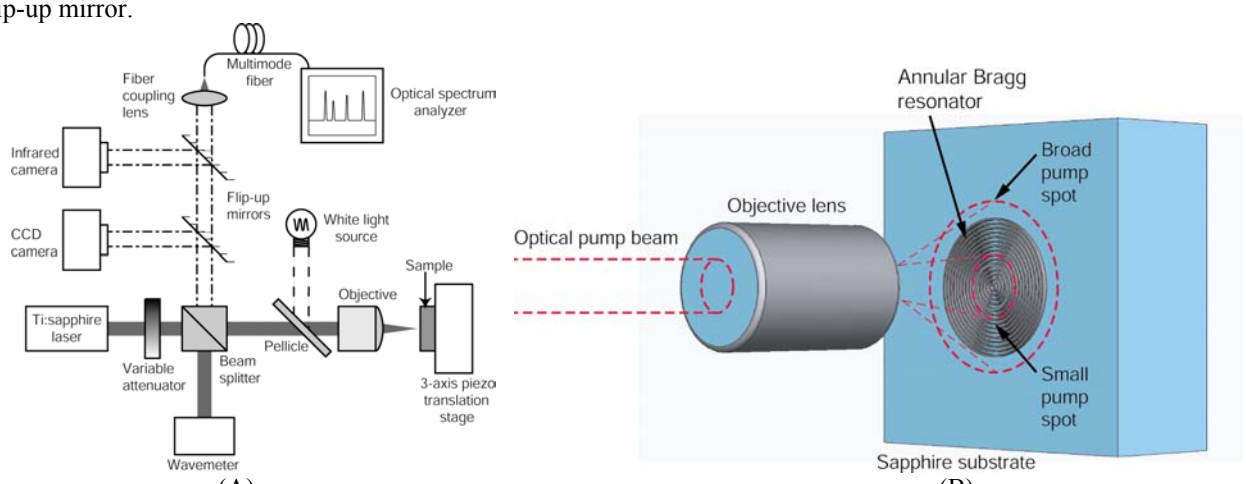

Figure 9. (A) Schematic of measurement setup. The solid gray line denotes the pump laser beam, the dash-dotted line denotes the resonator luminescence signal, and the dashed line denotes the white light used for imaging devices. (B) Close-up view of resonator, illustrating the positioning/focusing of optical pump spot.

Figure 10 depicts the photoluminescence spectra of the un-patterned QW layer structure for different pumping powers. As the pumping power is increased, the FWHM of the luminescence broadens from approximately 70nm to 110nm, and the peak of the photoluminescence shifts towards longer wavelength due to heating. The luminescence peak wavelengths at 5mW and 1mW pump level are essentially identical, indicating that heating is of less significance at these pump levels.

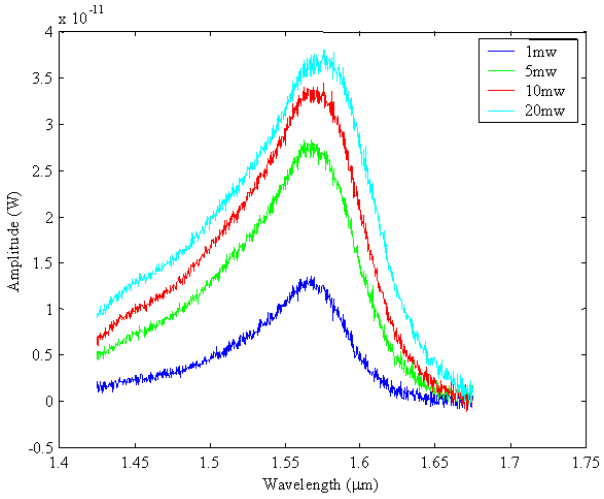

Figure 10. Photoluminescence of the unpatterned QW layer structure.

Figure 11 shows the spectra of an ABR with a $\lambda/2n$ defect (see Figure 8(A)) at low (Figure 11(A)) and high (Fig. 11(B)) pump levels. The inset of Figure 11(A) depicts the integrated spectral power emitted from the resonator surface, indicating lasing threshold at approximately 1mW pump power.

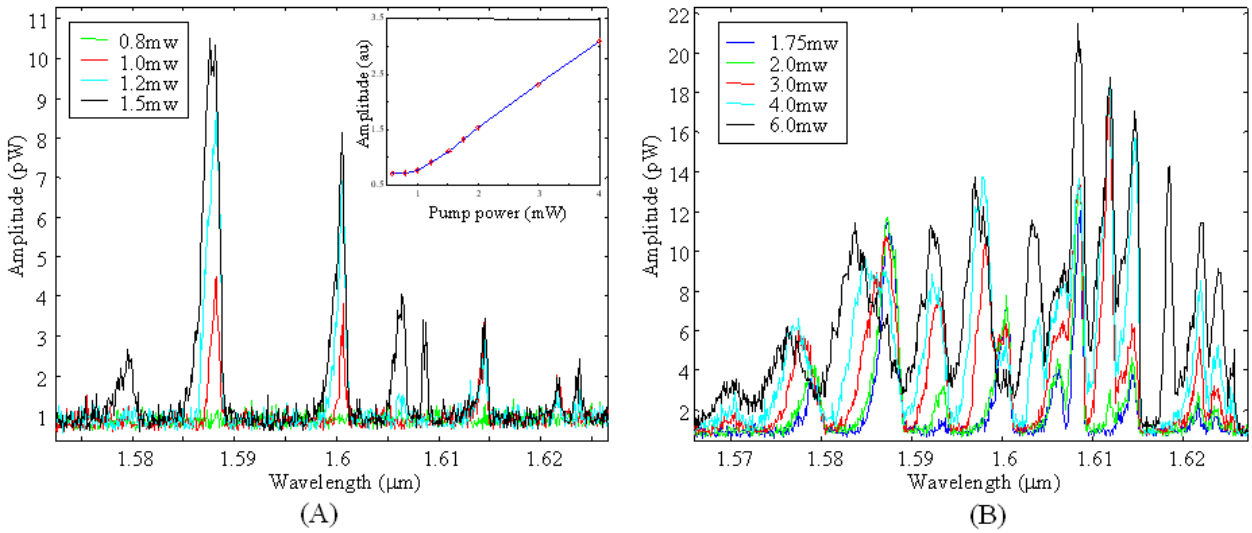

Figure 11. Emission spectra of an ABR (similar to the one shown in Figure 8(A)) for low (A) and high (B) pump powers. Inset in (A) – integrated emitted power as a function of the pumping level.

Just above threshold (Fig. 11(A)), the ABR exhibited four distinct resonance wavelengths with an FSR of approximately 14 nm. As the pump level was increased, the resonances broadened and slightly shifted towards shorter wavelengths. At higher pump levels (more than 1.5mW) emission in additional resonance wavelengths is shown. We attribute these resonances to more lossy modes which are not necessarily confined at the defect. As for the lower pump levels, the peaks continued to shift toward shorter wavelengths as the pump level was increased (see Figure 11(B)).
Theoretical analysis of the measured structure predicts an FSR of ~18 nm at (see Table 1). We attribute the difference between the theoretical and the measured FSRs to dimensions and refractive index differences and to the employment of the effective index approximation.

Azimuthal number	Wavelength (μm)
24	1.6325
25	1.613
26	1.5948
27	1.5769

Table 1. Theoretically calculated resonance wavelengths of the measured ABR.

6. CONCLUSIONS

We have analyzed annular defect mode ring resonators based on radial Bragg reflectors. We saw that extremely small resonators (a few microns in diameter) exhibiting large FSR can be realized utilizing relatively low index materials. Several geometries for the Bragg reflectors were suggested, analyzed and fabricated. The straightforward configuration (each layer serves as an equivalent quarter wavelength plate) offers the smallest resonator exhibiting the largest FSR. However, manufacturing of such a device requires the realization of small and accurate features, especially if the optimal grating structure is required. Employment of higher-order Bragg gratings relaxes the fabrication tolerances, but deteriorates the FSR.

The composite configuration, i.e. tailoring each layer's Bragg order and width according to its refractive index and radius, seems to be the best compromise between large FSR and fabrication complexity. Quarter wavelength layers can be easily realized if the material refractive index is low or if the layer is positioned in a small radius where the equivalent

index, n_{eq}, is low. Employing the thinnest possible Bragg layers is important especially for the internal Bragg reflector, because this region limits the minimum defect radius, and hence, the FSR. The external Bragg reflector could be realized using higher-order Bragg layers without a major influence on the resonator performance.

Several annular Bragg resonator designs, having varying defect order and azimuthal number *m*, were realized in an InGaAsP membrane structure. Electron beam lithography and several reactive ion etching steps were employed to define the resonator devices. A low-index UV curable optical adhesive was used to transfer the 250nm thick InGaAsP membrane to a sapphire substrate for improved optical confinement of the resonator modes. This epitaxial transfer process also facilitates the use of annular Bragg resonators in sensing applications, by permitting the optical near-field to interact with the surrounding environment from one side, while simultaneously allowing optical pumping and imaging of the photoluminescence signal through the transparent substrate.

The vertical emission from optically pumped ABRs was measured and analyzed. In-plane lasing was observed at 1.6μm with pump threshold of approximately 1mW. At low pump level, where membrane heating is insignificant, the resonance wavelengths tend to shift toward shorter wavelengths as the pumping is increased. Qualitative agreement was found between the spectral characteristics of the measured device and the two-dimensional theoretical analysis. Close to threshold, wide FSR of 14nm was exhibited. However, as the pumping power was increased, additional resonances appeared.

ACKNOWLEDGMENTS

The authors thank G. T. Paloczi, Y. Huang, J. K. S. Poon and J. M. Choi for useful discussions. In addition, the authors would like to acknowledge Dr. Axel Scherer and Dr. Oskar Painter for use of fabrication facilities. This research was supported by the U.S. Office of Naval Research and DARPA.

REFERENCES

1. E. A. J. Marcatili, "Bends in Optical Dielectric Guides", AT&T Tech. J. **48**, 2103-2132, 1969.
2. C. K. Madsen and J. H. Zhao, "*Optical Filter Design and Analysis: A Signal Processing Approach*", Wiley-Interscience Publications, New-York 1999, and references therein.
3. R. E. Boyd and J. Heebner, "Sensitive Disk Resonator Photonic Biosensor" Appl. Opt. **40**, 5742-5747, 2001.
4. J. Scheuer and A. Yariv, "Two-Dimensional Optical Ring Resonators Based on Radial Bragg Resonance", Opt. Lett. **28**,1528-1530, 2003.
5. J. Scheuer and A. Yariv, "Annular Bragg Defect mode Resonators", J. Opt. Soc. Am. B. **20**, 2285-2291, 2003.
6. J. Scheuer and A. Yariv, ″Optical Annular Resonators Based on Radial Bragg and Photonic Crystal Reflectors″, Opt. Express **11**, 2736-2746, 2003.
7. M. Toda, "Single-Mode Behavior of a Circular Grating for Potential Disk-Shaped DFB Lasers", IEEE J. Quantum Electron., **26**, 473-481, 1990.
8. X. H. Zheng and S. Lacroix, "Mode Coupling in Circular-Cylindrical System and Its Application to Fingerprint Resonators", IEEE J. Lightwave Technol., **8**, 1509-1516, 1990.
9. T. Erdogan and D. G. Hall, "Circularly Symmetric Distributed Feedback Laser: An analysis", J. Appl. Phys., vol. 68, p. 1435-1444, 1990.
10. T. Erdogan and D. G. Hall, "Circularly Symmetric Distributed Feedback Laser: Coupled Mode Treatment of TE Vector Fields", IEEE J. Quantum Electron. **28**, 612-623, 1992.
11. M. A. Kaliteevski, R. A. Abram, V. V. Nikolaev and G.S. Sokolovski, "Bragg reflectors for cylindrical waves", J. Mod. Optics **46**, 875-890, 1999.
12. C. Wu, M. Svilans, M. Fallahi, T. Makino, J. Glinski, C. Maritan and C. Blaauw, "Optically Pumped Surface-Emitting DFB GaInAsP/InP Lasers With Circular Grating", Electron. Lett. **27**, 1819-1821, 1991.
13. D. Labilloy, H. Benisty, C. Weisbuch, T. F. Krauss, C. J. M. Smith, R. Hourdré and U. Oesterle, "High-finesse disk microcavity based on a circular Bragg reflector", Appl. Phys. Lett. **73**, 1314-1316, 1998.
14. A. Shaw, B. Roycroft, J. Hegarty, D. Labilloy, H. Benisty, C. Weisbuch, T. F. Krauss, C. J. M. Smith, R. Stanely, R. Hourdré and U. Oesterle, "Lasing properties of disk microcavity based on circular Bragg reflector", Appl. Phys. Lett. **75**, 3051-3053, 1999.
15. D. Ochoa, R. Hourdré, M. Ilegems, H. Benisty, T. F. Krauss and C. J. M. Smith, "Diffraction of cylindrical Bragg reflectors surrounding an in-place semiconductor microcavity:, Phys. Rev. B **61**, 4806-4812, 2000.
16. S. Kim, H. Ryu, H. Park, G. Kim, Y. Choi, Y. Lee and J. Kim, "Two-dimensional photonic crystal hexagonal waveguide ring laser", Appl. Phys. Lett., vol. 81, p. 2499-2501, 2002.
17. See for example, A. Yariv, "*Optical Electronics in Modern Communications*" 5th ed., Oxford University Press, New-York, 1997.
18. P. Yeh, A. Yariv and E. Marom, "Theory of Bragg fiber", J. Opt. Soc. Am. **68**, 1196-1201, 1978.
19. Y. Xu, R. K. Lee and A. Yariv, "Asymptotic analysis of Bragg fibers", Opt. Lett. **25**, 1756-1758, 2000.
20. S. G. Johnson, M. Ibanescu, M. Skorobogatiy, O. Weisberg. T. D. Engeness, M. Soljačić, S. A. Jacobs, J.D. Joannopoulos and Y. Fink, "Low-loss asymptotically single-mode propagation in large-core OmniGuide fibers", Opt. Express **9**, 748-779, 2001.
21. G. Meltz, W. W. Morey and W. H. Glenn, "Formation of Bragg gratings in optical fibers by a transverse holographic method", Opt. Lett. **14**, 823-825, 1989.
22. L. A. Coldren and S. W. Corzine, "*Diode Lasers and Photonic Integrated Circuits*", Wiley-Interscience Publications, New York, 1995.
23. A. Marcuse, "*Theory of Dielectric Optical Waveguides*" 2nd ed., Academic Press, San Diego, 1991.
24. R. K. Lee, O. Painter, B. Kitzke, A. Scherer and A. Yariv, "Emission properties of a defect cavity in a two-dimensional photonic bandgap crystal slab", J. Opt. Soc. Am. B. **17**, 629-633, 2000.